Polymer 234 (2021) 124244

Contents lists available at ScienceDirect

Polymer

journal homepage: www.elsevier.com/locate/polymer

Light-promoted synthesis of surface-grafted polymers bearing pyridine groups by metal-free ATRP in microliter volumes

Monika Słowikowska [1], Artur J. Wójcik [1], Karol Wolski [*], Anna Hatalak, Szczepan Zapotoczny

Faculty of Chemistry, Jagiellonian University, Gronostajowa 2, 30-387, Krakow, Poland

ARTICLE INFO

Keywords:
Metal-free ATRP
Polymer brushes with pyridine groups
pH responsive materials

ABSTRACT

Polymers with pendant pyridine groups (PPPGs) are pH responsive weak polyelectrolytes potentially attractive for many applications such as sensors, antibacterial coatings, and ion gating systems. Synthesis of PPPGs by classical atom transfer radical polymerization (ATRP) is very challenging due to highly probable formation of monomer/metal complexes. In response to that, we report here a facile synthetic strategy to obtain surface-grafted PPPGs that utilizes light-mediated ATRP. Metal-free surface-initiated ATRP catalyzed by 10-phenylphenothiazine is used to polymerize three isomeric monomers with methacrylate groups attached at various positions of a pyridine ring. The reactivity of the isomers is compared for selection of optimal monomer structure leading to thick brushes. The polymerizations are conducted under visible light, at ambient conditions, and using only microliter volumes of the reaction mixture that is important for reducing the complexity and costs of the process as well as limiting chemical waste. The observed linear dependency of the brush thickness vs polymerization time for poly(pyridin-3-yl methacrylate) (PP3M) grafted from indium tin oxide or silicon wafers indicated the controlled characteristics of the developed method. The obtained PP3M brush demonstrated pH responsive behavior associated with protonation of pyridine groups in acidic solution and adoption of highly stretched conformation below pK_a.

1. Introduction

Polymers with pendant pyridine groups (PPPGs) are in the field of interest of many scientific groups around the world, due to their desired characteristics: ability to coordinate transition metal ions [1], pH sensitivity [2] and easy functionalization by quaternization of the pyridine ring [3,4]. All these features makes them a perfect candidates for numerous applications such as: drug delivery systems [5], platforms for controlled adsorption of proteins [6], filtration systems [7], ion gating membranes [8], dye-sensitized solar cells [9], sensors [10], antibacterial agents [11] and catalysts [12].

In case of some of the abovementioned applications it is highly desirable to form a stable coating with covalent attachment of the chains to various substrates. This can be realized by formation of surface-grafted polymer brushes by "grafting to" or "grafting from" technique [13]. However, only the second approach enables formation of well-defined layers with adjustable thicknesses and grafting densities spanning a broad range. Within this approach, commonly surface-initiated reversible deactivation radical polymerizations (SI-RDRP) were used to graft PPPGs on various substrates such as: indium tin oxide (ITO) [4], nanoparticles [14], polymer membranes [15], graphene oxide [16], nanorods [17] or cellulose [18]. The most frequently reported technique for production of PPPGs brushes via "grafting from" is surface-initiated atom transfer radical polymerization (SI-ATRP) [13]. However, SI-ATRP of commercially available pyridine-based monomers such as: 4-vinylpyridine (4VP), 3-vinylpyridine (3VP), 2-vinylpyridine (2VP) is significantly hindered, due to strong ability of pyridine groups to form complexes with copper catalysts [19]. Pyridine-based monomers as well as PPPGs are strong coordinating ligands that can compete with ligands forming activation complexes with copper or other transition metals [20]. Monomers are generally used in huge excess with respect to ATRP ligands, hence formation of monomer/metal complexes is highly probable, which may limit the polymerization rate. Matyjaszewski et al. have found that addition of only 5% (by volume) of pyridine significantly slowed down the ATRP polymerization (in solution) of styrene catalyzed by CuBr/4, 4′-di-(5-nonyl)-2,2′-bipyridine complex [21]. In case of ATRP of 4VP in the solution, the improved rate and dispersity were observed when

* Corresponding author.
E-mail address: wolski@chemia.uj.edu.pl (K. Wolski).
[1] These authors contributed equally to this work.

https://doi.org/10.1016/j.polymer.2021.124244
Received 22 June 2021; Received in revised form 8 September 2021; Accepted 2 October 2021
Available online 4 October 2021

strong coordinating and active ligands such as Me_6TREN were used to form complexes with CuCl [20]. However, it is worth to mention that even Me_6TREN used with CuBr did not provide optimal conditions, due to enhanced termination reactions.

In case of synthesis of the brushes by SI-ATRP the mentioned problems seem to play even more important role as most of the papers presenting synthesis of PPPGs brushes reported formation of the layers thinner than 20 nm [17,22] [–] [25]. However, Saha et al. reported formation of very thick poly(4-vinylpyridine) (P4VP) brushes (~200 nm) on both silicon and gold surface, but analysis of the dependency of layer thickness vs polymerization time, suggests that polymerization was not fully controlled [26]. Raczkowska et al. presented synthesis of thick P4VP brushes (42 nm) using SI-ATRP with activator regenerated by electron transfer (SI-ARGET-ATRP) indicating successful utilization of ATRP methods with reduced concentration of transition metal complexes [27]. Recently, it was shown that controlled SI-ATRP of various monomers could be conducted in the presence of ppm amounts of metal catalyst [28] [–] [30] or in metal-free conditions by replacing classical transition metal complex with organic photoactive molecule [31,32]. The second approach seems to be especially very attractive in terms of polymerization of pyridine-based monomers as metal complexes could be excluded from the reaction mixture. Indeed Ma et al. showed that P4VP could be grafted from graphene oxide by metal-free SI-ATRP in the presence of sacrificial initiator and 10-phenylphenothiazine (PTH) under UV light [33]. However, in 2018, Narupai et al. showed that metal-free SI-ATRP catalyzed by PTH could be even more powerful enabling polymerization of various methacrylic monomers in microliter volumes only (saving reactant), under visible light and ambient conditions [34]. PTH is a singlet excited state reductant, therefore its deactivation by triplet-triplet annihilation with oxygen is limited [35]. Moreover, PTH in the excited states may react with oxygen-derived free radicals converting them to oxygen [35], thus metal-free ATRP in solution could be performed even at ambient conditions [36]. Inspired by these works, we aimed to use metal-free SI-ATRP for synthesis of three different surface-grafted PPPGs from silicon wafer or ITO surface. We synthesized three methacrylic monomers with pendant pyridine groups: pyridin-4-yl methacrylate (P4M), pyridin-3-yl methacrylate (P3M) and pyridin-2-yl methacrylate (P2M) and compared their reactivity. All polymerizations were mediated by visible light (λ_{max} = 405 nm) and conducted in microliter volumes demonstrating tolerance to ambient conditions.

2. Experimental section

2.1. Materials

Silicon wafers were obtained from ON Semiconductor (Roznov, Czech Republic). ITO substrates (glass slides covered with 100 nm thick layer of ITO) were purchased from Osilla (Sheffield, UK). Cover slips of the size 24 × 24 mm were obtained from Heinz Herenz (Hamburg, Germany). 2-hydroxypyridine (98%), 3-hydroxypyridine (98%), 4-hydroxypyridine (97%), phenothiazine (min. 98%), 1,4-dioxane (dried, min. 99.8%) and molecular sieves (3A) were purchased from Alfa Aesar (Haverhill, MA, USA). Methacryloyl chloride (95%, 200 ppm MEHQ as stabilizer), chlorobenzene (anhydrous, min. 99.8%) and sodium tert-butoxide (99%, pure) were purchased from Acros Organics (Geel, Belgium). RuPhos was obtained from Ark Pharm (IL, USA). RuPhos Pd G2 precatalyst, (3-aminopropyl)triethoxysilane (APTES, 99%), α-bromoisobutyryl bromide (BIB, 98%), ethyl α-bromophenylacetate (EBPA, 97%), acetonitrile (HPLC, ≥99.9%) were purchased from Sigma-Aldrich (St Louis, MO, USA). Triethylamine (min. 99.0%) was obtained from TCI Chemicals (Tokyo, Japan). Dichloromethane (min. 99.5%, p.a.), n-hexane (min. 99.0%, p.a.), ethyl acetate (min. 99.5%, p.a.), methanol (min. 99.8%, p.a.), ethanol (96%, p.a.) sodium sulfate (anhydrous, min. 99.0%, p.a.), hydrogen peroxide (30%, p.a.), ammonium solution (25%, p.a.), sulfuric acid (96%, p.a.), toluene (p.a.), sodium chloride (min. 99.8%, p.a.) and hydrochloric acid (35–38%, p.a.) were all purchased from Chempur (Piekary Śląskie, Polska). Ammonium chloride (pure) was purchased from POCH Avantor Performance Materials (Gliwice, Poland). Silica gel (LC 60, 70–200 mesh) and *N*,*N*-dimethylacetamide (DMAc, 99%) were obtained from Fluorochem (Hadfield, UK). Methacryloyl chloride was distilled whereas dichloromethane and *N*,*N*-dimethylacetamide were dried over molecular sieves before usage. Rest of chemicals were used as received.

2.2. Methods

LED lamp emitting at 405 nm (M405LP1, Output Power 1200–1700 mW, Thorlabs, Newton, MA, USA) equipped with a heat sink was used for metal-free SI-ATRP (see Fig. S1). The light intensity used for polymerization was set to 130 W/m^2 (measured by the Delta OHM HD2302.0 light meter equipped with the probe sensitive for the spectral range 400–1050 nm). Atomic force microscopy (AFM) images were obtained using Dimension Icon AFM (Bruker, Santa Barbara, CA, USA). AFM was operating in the PeakForce QNM® mode. ScanAsyst-air probes with a nominal spring constant of 0.4 N/m were used for topography measurements in air, while biosphere B300-FM probe (tip radius 300 ± 10 nm, Nanotools, München, Germany) was used for measurements in liquids. The spring constant of the B300-FM probe (4.67 ± 0.2 N/m) was calibrated by the thermal-noise method. The deflection sensitivity of the optical beam-detection system was calibrated on nondeformable sapphire glass surface. To measure the brush thickness, the samples were scratched gently by needle, rinsed with copious amount of THF, ultrasonicated in toluene (5 min), and then, the AFM images were captured in an ambient air or solution at the edge of the scratch. The average dry thicknesses were determined from depth histograms acquired from height images captured at several locations on each sample. In case of thickness measurements at different pH and in acetonitrile, all the measurements were performed in one place at nearly the same position. The GA-FTIR spectra of the brushes grafted from ITO surface were recorded using a Thermo Nicolet iS10 FT-IR spectrometer with a grazing-angle reflectance accessory (at an incident angle of 80°) using a p-polarized beam. All the spectra were averaged from 256 scans and baseline corrected using Omnic Software. The FTIR spectra of the monomers (see the SI) were captured using the same spectrometer equipped with an ATR accessory (SMART iTX). ^{1}H and ^{13}C NMR spectra were recorded on a Bruker Avance III 400 MHz spectrometer. Chemical shifts are reported in ppm relative to the deuterated solvent resonance. LCMS analysis was performed employing an analytical set of an ultra-high performance liquid chromatography from Dionex UltiMate 3000 with a UV–Vis detector coupled with a high-resolution mass spectrometer with a time-of-flight analyzer (ESIQTOF) – Bruker Impact II. A gradient method was used (column: Gemini NX – C18, 150 × 3.0, 3 μm 110 A; phase A: H_2O MS + formic acid (0.1%); phase B: acetonitrile MS + formic acid (0.1%)). Only the positive ionization method gave results. Static contact angles measurements were performed for PP3M and PMMA brushes grafted on silicon wafers using a video-based optical contact angle instrument (OWIS) at room temperature using Surftens 3.0 software. To measure the contact angle at different pH, 12 solutions of hydrochloric acid with pH ranging from 0.42 to 5.29 were prepared by mixing an appropriate amount of hydrochloric acid with deionized water. The 5 μl droplets of DI water or hydrochloric acid solutions were placed carefully on the PP3M or PMMA brush sample. The contact angles were measured after 2 and 5 min of incubation, in 2 different positions; at each position, the measurement was performed 5 times. After each measurement, the samples were rinsed with DI water and dried under a stream of nitrogen. Gel permeation chromatography (GPC) analysis of polymer samples was performed using a Shimadzu modular system comprising of a CBM-40 system controller, an SIL-20AHT automatic injector, with one precolumn and three 10 μm columns (pore size: 100 Å, 3000 Å and 3000 Å, PSS Polymer), RID-20A differential refractive-index detector. The temperature of the columns was

maintained at 30 °C using a CTO-20A oven. The eluent was *N*,*N*-dimethylformamide (HPLC grade, with 0.01 M LiCl) and the flow rate was kept at 1 mL/min using an LC-40 pump. A molecular weight calibration curve was produced using commercial narrow molecular weight distribution polystyrene standards.

Synthesis of the brushes by metal-free SI-ATRP. The initiator decorated ITO or SiO_2 substrates were prepared in a twostep process by grafting APTES-BIB ATRP initiator according to the previously reported procedure [37]. The thickness of APTES-BIB initiator layer (2.2 ± 0.2) was determined on SiO_2 surface by spectroscopic ellipsometry. P2M, P3M or P4M solutions with the concentration of either 2.1 or 1.4 M in DMAc were prepared in small amber vials sealed with rubber septa under argon atmosphere. The amount of PTH used in all reactions was set to 1 mol% with respect to the monomer, while the total volume of stock polymerization mixture was 200 μL. In order to run the polymerization on a single plate, a drop of reaction mixture (typically 20–30 μL) was placed in air on top of initiator modified ITO or SiO_2 substrate and then covered with the glass plate forming homogeneously distributed thin layer of polymerization solution. The polymerization was initiated by exposing the samples to LED light (λ_{max} = 405 nm) at ambient conditions (see Fig. S1). For comparing the reactivity of the synthesized monomers all the reaction conditions were kept constant and the time of polymerization was set to 4 h. In case of kinetic studies of PP3M brushes, reaction time was varied from 1 to 4 h. After polymerization, the samples were rinsed by copious amount of DMAc, ultrasonicated in DMAc, THF and toluene (10 min in each solvent) and finally dried under stream of argon.

Metal-free ATRP in solution. The molar ratios of the reagents used in the reactions were as follows: [monomer]/[EBPA]/[PTH] = 100/1/1. The polymerization mixture was prepared in the dark, in an argon-purged system consisting of amber glass vessel connected with double-tipped needle with specially designed polymerization vessel sealed with a rubber septum. P2M, P3M or P4M polymerization solutions with the concentration of 2.1 M in DMAc were prepared in an amber vial (total reaction volume 1 mL) and then transferred to the polymerization vessel with EPBA and magnetic stirring bar inside. The vessel was placed on magnetic stirrer and exposed to LED light (λ_{max} = 405 nm) at room temperature (light intensity was the same as in the case of metal-free SI-ATRP). Small portions of the reaction mixture were collected after given time to determine apparent number average molecular weight M_n^{app} and dispersity (M_w^{app}/M_n^{app}) by means of GPC measurements and monomer conversion using ^{1}H NMR.

Synthesis of pyridin-2-yl *methacrylate (P2M).* A mixture of 2-hydroxypyridine (1.136 g, 11.94 mmol, 1.00 equiv) and triethylamine (2.11 mL, 15.2 mmol, 1.27 equiv) in dried dichloromethane (22.8 mL) was stirred at 0 °C under argon atmosphere for 30 min. Methacryloyl chloride (1.32 mL, 13.5 mmol, 1.13 equiv) was then added dropwise during 60 min. The reaction was carried out for 4 h at room temperature. The reaction progress was controlled by means of TLC: *n*-hexane/ethyl acetate 2/3 v/v, $R_{f,\ product}$ = 0.7. The reaction mixture was washed with a saturated aqueous solution of ammonium chloride (2 × 20 mL) and then with deionized water (2 × 20 mL). A desired product which remained partially in combined aqueous layers was extracted with dichloromethane (3 × 30 mL). Resulting organic layers were combined and dried over anhydrous sodium sulfate, filtered, and concentrated under vacuum (max. 30 °C, 2 mbar). The crude product was purified through a column chromatography over silica gel (*n*-hexane/ethyl acetate 92/8 -> 84/16 v/v) leading to a colorless oil (1.845 g, 94.70% yield).

^{1}H NMR (400 MHz, $CDCl_3$, δ/ppm) (Fig. S2): δ = 8.41 (1H, ddd, J = 4.9, 1.9, 0.5 Hz), 7.79 (1H, ddd, J = 8.1, 7.4, 2.0 Hz), 7.22 (1H, ddd, J = 7.4, 4.9, 0.9 Hz), 7.10 (1H, dt, J = 8.1, 0.9 Hz), 6.40 (1H, quint, J = 1.0 Hz), 5.79 (1H, quint, J = 1.4 Hz), 2.06 (3H, dd, J = 1.4, 1.0 Hz). ^{13}C NMR (101 MHz, $CDCl_3$, δ/ppm) (Fig. S3): δ = 165.6, 158.3, 148.7, 139.6, 135.6, 128.2, 121.1, 116.7, 18.4. FTIR (ν~/cm^{-1}) (Fig. S4): ~3030 (weak, ν(C–H)$_{arom.}$), 2928 (ν(–CH$_2$)$_{asym}$), 1735 (ν(C═O)), 1637 (ν(C═C)), 1591, 1573 (ν(C═C) or ν(C═N)), 1112 (ν(C–O)). ESI-HRMS (Fig. S5, positive ion mode): *m/z* calculated for [M+H]+ amounts 164.1806; found 164.0707.

Synthesis of pyridin-3-yl *methacrylate (P3M).* A mixture of 3-hydroxypyridine (3.28 g, 34.5 mmol, 1.00 equiv) and triethylamine (8.42 mL, 60.4 mmol, 1.75 equiv) in anhydrous dichloromethane (65.7 mL) was stirred at 0 °C under argon atmosphere for 15 min. Methacryloyl chloride (3.56 mL, 36.4 mmol, 1.06 equiv) was added dropwise during 30 min. The reaction was carried for 2 h at room temperature. The reaction progress was controlled by means of TLC: *n*-hexane/ethyl acetate 1/1 v/v, $R_{f,\ product}$ = 0.5. The reaction mixture was washed with a saturated aqueous solution of ammonium chloride (2 × 50 mL) and then with deionized water (1 × 50 mL). A desired product which remained partially in combined aqueous layers was additionally extracted with dichloromethane (2 × 50 mL). The resulting organic layers were combined and dried over anhydrous sodium sulfate, filtered, and concentrated under vacuum (max. 35 °C, 2 mbar). The crude product was purified through a column chromatography over silica gel (*n*-hexane/ethyl acetate 100/0 -> 84/16 v/v) leading to a colorless oil (5.0 g, 88.8% yield).

^{1}H NMR (400 MHz, $CDCl_3$, δ/ppm) (Fig. S6): δ = 8.49 (1H, dd, J = 4.7, 1.4 Hz), 8.46 (1H, d, J = 2.7 Hz), 7.51 (1H, ddd, J = 8.4, 2.7, 1.4 Hz), 7.34 (1H, dd, J = 8.4, 4.7, 0.5 Hz), 6.38 (1H, quint, J = 0.9 Hz), 5.81 (1H, quint, J = 1.4 Hz), 2.07 (3H, dd, J = 1.4, 0.9 Hz). ^{13}C NMR (101 MHz, $CDCl_3$, δ/ppm) (Fig. S7): δ = 165.28, 147.59, 146.86, 143.49, 135.29, 129.25, 128.11, 123.83, 18.31. FTIR (ν~/cm^{-1}) (Fig. S8): ~3030 (weak, ν(C–H)$_{arom.}$), 2929 (ν(–CH$_2$)$_{asym}$), 1734 (ν(C═O)), 1637 (ν(C═C)), 1578 (ν(C═C) or ν(C═N)), 1114 (ν(C–O)). ESI-HRMS (Fig. S9, positive ion mode): *m/z* calculated for [M+H]+ amounts 164.1806; found 164.0707.

Synthesis of pyridin-4-yl *methacrylate (P4M).* A mixture of 4-hydroxypyridine (1.317 g, 13.85 mmol, 1.00 equiv) and triethylamine (5.00 mL, 35.9 mmol, 2.59 equiv) in dried dichloromethane (26.3 mL) was stirred at 0 °C under argon atmosphere for 15 min. Methacryloyl chloride (2.30 mL, 23.5 mmol, 1.70 equiv) was added dropwise during 60 min. The reaction was carried out overnight at room temperature. The reaction progress was controlled by means of TLC: dichloromethane/methanol 4/1 v/v, $R_{f,\ product}$ = 0.9. The reaction mixture was washed with a saturated aqueous solution of ammonium chloride (2 × 20 mL) and then with deionized water (2 × 20 mL). A desired product which remained partially in combined aqueous layers was extracted with dichloromethane (3 × 40 mL). The resulting organic layers were combined and dried over anhydrous sodium sulfate, filtered, and concentrated under vacuum (max. 30 °C, 5 mbar). The crude product was purified through a column chromatography over silica gel twice (first and second purification: *n*-hexane/ethyl acetate 100/0 -> 80/20 v/v) leading to yellow oil (1.103 g, 48.81% yield).

^{1}H NMR (400 MHz, $CDCl_3$, δ/ppm) (Fig. S10): δ = 8.62 (2H, d, J = 4.7 Hz), 7.14 (2H, d, J = 4.7 Hz), 6.36 (1H, quint, J = 0.9 Hz), 5.81 (1H, quint, J = 1.4 Hz), 2.05 (3H, dd, J = 1.4, 0.9 Hz). ^{13}C NMR (101 MHz, $CDCl_3$, δ/ppm) (Fig. S11): δ = 164.6, 157.8, 151.5, 135.4, 128.5, 117.1, 18.4. FTIR (ν~/cm^{-1}) (Fig. S12): 3075, 3050 (ν(C–H)$_{arom.}$), 2978 (ν(–CH$_3$)$_{asym.}$), 2939 (ν(–CH$_2$)$_{asym.}$ and ν(–CH$_3$)$_{sym.}$), 1741, 1703 (ν(C═O)), 1640 (ν(C═C) or ν(C═N)), 1585, 1531 (ν(C═C), 1121 (ν(C–O)), 752 (pyridine ring). ESI-HRMS (Fig. S13, positive ion mode): *m/z* calculated for [M+H]+ amounts 164.1806; found 164.0708.

Synthesis of 10-phenylphenothiazine (PTH). The procedure reported herein is modified version of the synthesis protocol described elsewhere [38]. Phenothiazine (0.423 g, 2.12 mmol, 1.00 equiv), sodium *tert*-butoxide (0.265 g, 2.76 mmol, 1.30 equiv), RuPhos (0.010 g, 0.021 mmol, 0.012 equiv) and RuPhos Pd G2 precatalyst (0.016 g, 0.021 mmol, 0.010 equiv) were added to a glass pressure tube. Dry dioxane (2.1 mL) and anhydrous chlorobenzene (0.280 mL, 2.76 mmol, 1.30 equiv) were added under argon. The tube was located in a microwave reactor and the reaction was carried out for 45 min (5 W, 46 psi, 110 °C). Upon cooling to room temperature, the reaction mixture was diluted with ethyl acetate (6 mL) and washed with a saturated aqueous solution of sodium chloride (2 × 4 mL) and then with distilled water (2 × 4 mL).

A desired product which remained partially in combined aqueous layers was additionally extracted with ethyl acetate (3 × 6 mL). The resulting organic layers were combined and dried over anhydrous sodium sulfate, filtered, and concentrated under vacuum (max. 30 °C, 5 mbar). The crude product was purified through a column chromatography over silica gel (*n*-hexane/ethyl acetate 99/1 -> 95/5 v/v) leading to a colorless crystalline solid (0.554 g, 94.9% yield).

^{1}H NMR (400 MHz, $CDCl_3$, δ/ppm) (Fig. S14): δ = 7.61 (2H, t, J = 7.7 Hz), 7.48 (1H, t, J = 7.4 Hz), 7.40 (2H, d, J = 8.4 Hz), 7.03 (2H, dd, J = 7.2, 1.9 Hz), 6.89–6.77 (4H, m), 6.21 (2H, dd, J = 7.9, 1.5 Hz). ^{13}C NMR (101 MHz, $CDCl_3$, δ/ppm) (Fig. S15): δ = 144.4, 141.2, 131.0, 130.9, 128.3, 127.0, 126.8, 122.6, 120.3, 116.2. FTIR ($\nu\sim$/cm^{-1}): 3059 (ν(C–H)$_{arom.}$), 1586, 1570 (ν(C═C)), 1490, 1463, 1443 (ν(C═C–C)), 1306, 1256 (ν(C–N)), 937, 899 (ν(C–S)). ESI-HRMS (Fig. S16): *m/z* calculated for [M]+ amounts 275.3675; found 275.0764.

3. Results and discussion

The monomers were synthesized in a one-step synthesis by reacting appropriate hydroxypyridines with methacryloyl chloride. The incorporation of methacrylate group in the monomer structure was dictated by its high reactivity and compatibility with metal-free SI-ATRP as indicated by Narupai et al. [34]. The structures of the obtained isomers: P4M, P3M and P2M (see Scheme 1) were confirmed by NMR, FTIR and ESI-HRMS spectroscopy (see experimental section and SI). The monomers were subjected to the same conditions of metal-free SI-ATRP to verify their reactivity as well as selecting the most promising compound for additional tests.

ITO or silicon wafers were at first modified with (3-aminopropyl) triethoxysilane (APTES) and then α-bromoisobutyryl bromide (BIB) forming APTES-BIB initiator according to the previously reported procedure [35]. Freshly prepared initiator decorated substrates were then immediately used for polymerizations. Metal-free SI-ATRP of the synthesized monomers was tested for two different concentrations of monomers (see Table 1). The polymerization mixture was composed of only monomer, PTH and solvent (DMAc, see Scheme 1). The concentration of PTH was set to 1 mol% with respect to monomer concentration while the total volume of the solution used for polymerization on a single plate was only 20–30 μL. In a typical process a drop of polymerization mixture (20–30 μL) was placed onto initiator decorated substrate (in air) which was then subsequently covered by coverslip. As a result, the thin layer of the reaction mixture was sandwiched between two flat surfaces. Such prepared samples were then exposed to LED light (λ_{max} = 405 nm) for a given time. The utilization of glass cover slip provided a barrier for oxygen diffusion. Besides formation of homogenous brush layers on the studied substrates, no brush grafting close to the border of the sample (the distance varied from 0.7 to 1.2 mm depending on the sample) was revealed (see Fig. S17). The observed edge effect was reported by the Hawker group and assigned to oxygen diffusion leading to decreased concentration of PTH close to the border of the sample [34]. Analyzing the results of brush thickness measurements (Table 1) one may conclude that P3M monomer is characterized by the highest reactivity. For each compound we observed an increase of brush thickness when using higher concentration of the monomer. However, in case of synthesis of poly(pyridin-2-yl methacrylate) (PP2M) brushes precipitation of polymer was observed at higher concentrations of monomer, indicating on occurring of polymerization in solution due to possible chain transfer reactions. It is also reflected in AFM topography images showing formation of less homogenous layer with visible spots and aggregates when compared to poly(pyridin-3-yl methacrylate) PP3M and poly(pyridin-4-yl methacrylate) PP4M brushes (Fig. 1). The arithmetic average roughness of PP2M surface, R_a = 7.4 nm, was substantially higher than that of PP3M, R_a = 2.5 nm, and PP4M, R_a = 2.2 nm. PP3M brushes were found to be the thickest in both polymerization conditions. The reactivity of the studied monomers was also compared by performing metal-free ATRP in the solution. The performed polymerizations revealed the same trend as in the case of metal-free SI-ATRP. The reactivity of the studied monomer increases in the order P4M < P2M < P3M but the observed differences in solution are even more pronounced (see Table S1). The best polymerization control (M_w^{app}/M_n^{app} = 1.54) was achieved for P3M. These results indicate that the position of methacrylate group with respect to the nitrogen atom in pyridine plays an important role influencing activation of the vinyl group or stabilization of the radical centers during polymerization. Pyridine-based monomers may also undergo S_N2 reactions with the terminal and initiating alkyl halide headgroups leading to the termination of the growing chains and formation of branched structures [20]. The probability of such reactions should be the highest in case of P4M monomer due to less steric hindrance compared to P2M and P3M as the methacrylate group is located in para position with respect to nitrogen atom in pyridine ring. Low reactivity of P4M could be also the result of some remaining impurities after synthesis, as monomer was slightly colored even after repeated purification procedure (P2M and P3M were colorless oils, see experimental section). It is worth emphasizing that differences in reactivity of 2VP and 4VP monomers were reported in case of RAFT [39], free radical polymerization and ATRP catalyzed by Cu(II) metal organic frameworks [40]. In case of RAFT and free radical polymerization, 2VP was found to be more reactive leading to formation of macromolecules with higher molar masses but also higher dispersity in case of the free

Table 1
Results of metal-free SI-ATRP of P2M, P3M and P4M.

Monomer	Monomer concentration (M)[a]	Dry thickness (nm)[b]
P2M	1.4	23 ± 1
	2.1	43 ± 1
P3M	1.4	28 ± 4
	2.1	58 ± 1
P4M	1.4	5 ± 1
	2.1	19 ± 1

[a] In all cases the reaction time was set to 4 h, and the monomer : PTH molar ratio was equal to 100 : 1.
[b] Dry thicknesses of the brushes grafted from ITO were measured by AFM.

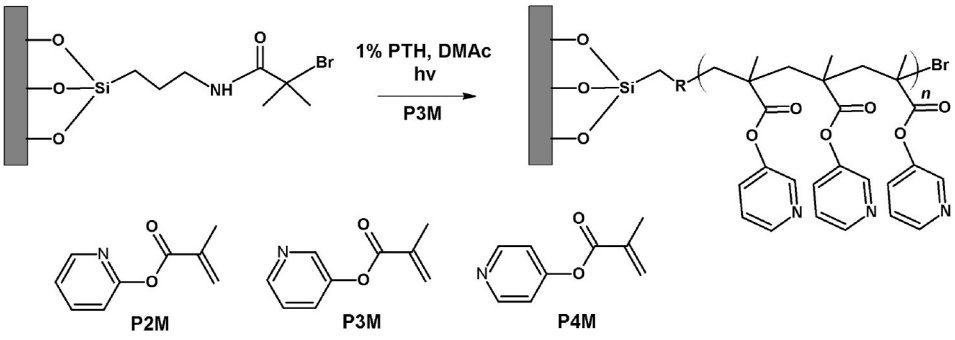

Scheme 1. Synthetic route to PPPGs brushes prepared by metal-free surface-initiated ATRP.

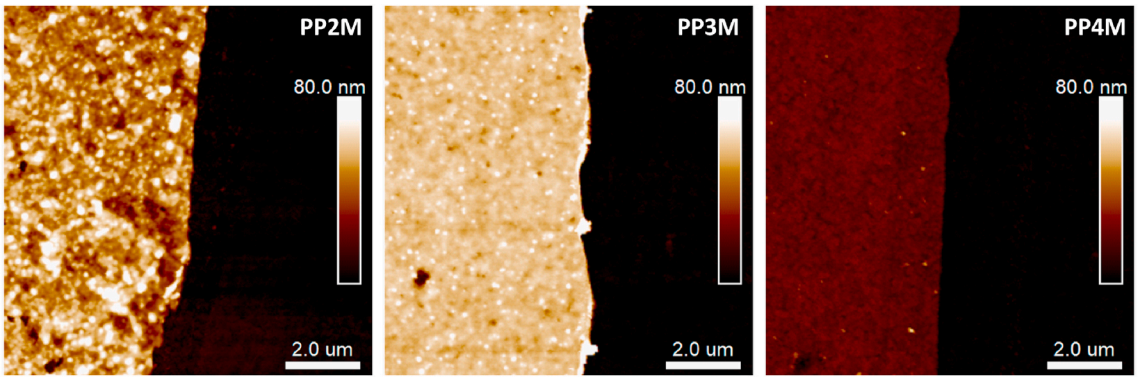

Fig. 1. AFM topography images of PP2M, PP3M and PP4M brushes obtained after 4 h of metal-free SI-ATRP from ITO surface (monomer concentration 2.1 M). The images are presented with the same height scale.

radical process [39,40]. It is in agreement with the presented results, as P2M monomer was found to be more reactive than P4M, but its polymerization is less controlled resulting in more heterogeneous layers. However, in case of ATRP catalyzed by Cu(II) metal organic frameworks faster polymerization was observed for 4VP that was assigned to stronger coordination of metal centers by 4VP (in this case it has positive effect) allowing enhanced light triggered reduction of Cu(II) to Cu(I) [40].

The chemical structure of the synthesized brushes was analyzed by Grazing-Angle Reflectance Fourier Transform Infrared Spectroscopy (GA-FTIR) (see Fig. 2). The spectra were measured for the brushes prepared at higher concentration of the monomers. The absorption intensity in GA-FTIR spectrum is proportional to total polymer mass on the surface [41,42]. Therefore, the observed absorption intensities increase in a row: PP4M, PP2M and PP3M, which is in agreement with the obtained thicknesses (Table 1). For each sample typical bands for pyridine ring were detected: C–H stretching vibration in aromatic ring (above 3000 cm^{-1}), C═C and C═N stretching vibrations (1470-1595 cm^{-1}), carbonyl group: C═O stretching (around 1760 cm^{-1}), C–O–C stretching (1100-1215 cm^{-1}) as well as polymer main chain: C–H stretching in aliphatic groups (slightly below 3000 cm^{-1}), C–H bending (1380-1450 cm^{-1}).

For further studies we have selected P3M monomer, due to the best performance in metal-free SI-ATRP. In order to verify the controlled character of the metal-free SI-ATRP in the case of metal-complexing PPPGs, the dependence of PP3M layer thickness vs time of polymerization was evaluated (see Fig. 3). In order to show the versatility of this method the kinetics of brush growth was followed on both ITO and silicon wafers. The choice of ITO was motivated by its high conductivity and transparency which is desirable for certain applications of PPPGs e.g., photovoltaic solar cells [43], organic light emitting diodes [10] or sensors [44]. The polymerizations were performed without sacrificial initiator in the solution, hence the linear dependency of brush thickness vs polymerization time was expected. Indeed, linear brush growth was observed up to 4 h of polymerization for the layers grafted from both ITO and silicon wafers pointing to controlled characteristics of the process. The polymerization slows down after 4 h likely due to some side reactions, while the maximum brush thickness (66 ± 5 nm in case of ITO) could be achieved after 6 h. When comparing the kinetics of metal-free ATRP of P3M in solution with metal-free SI-ATRP one may observe some differences. Although, the linear dependency in semilogarithmic kinetic plot (see Figure S18B) is observed pointing to stable concentration of propagating radical centers, the dependency of molecular weight vs monomer conversion slightly deviates from linear characteristics (Figure S18A) as reported previously for metal-free ATRP of other monomers [45]. The obtained M_n^{app} values are higher than theoretical molecular weights (M_n^{th}) pointing to low initiation efficiency or overestimation of molar masses due to applied polystyrene standards in GPC measurements [45].

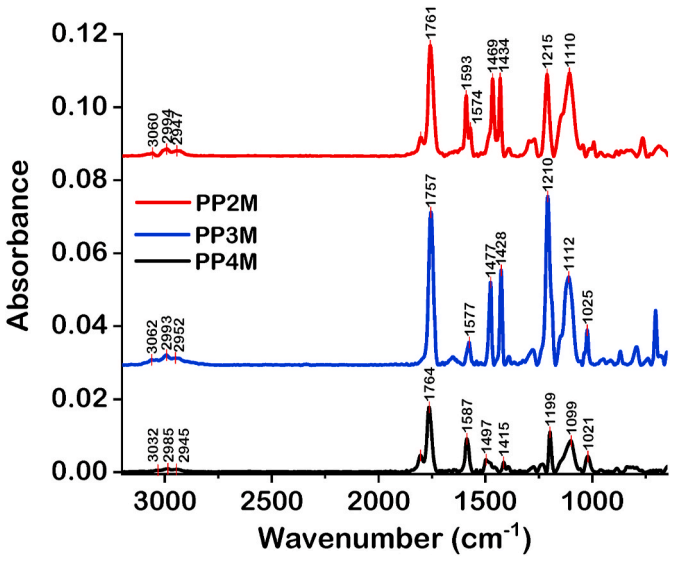

Fig. 2. GA-FTIR absorbance spectra of PP2M, PP3M and PP4M. The spectra are vertically offset for clarity.

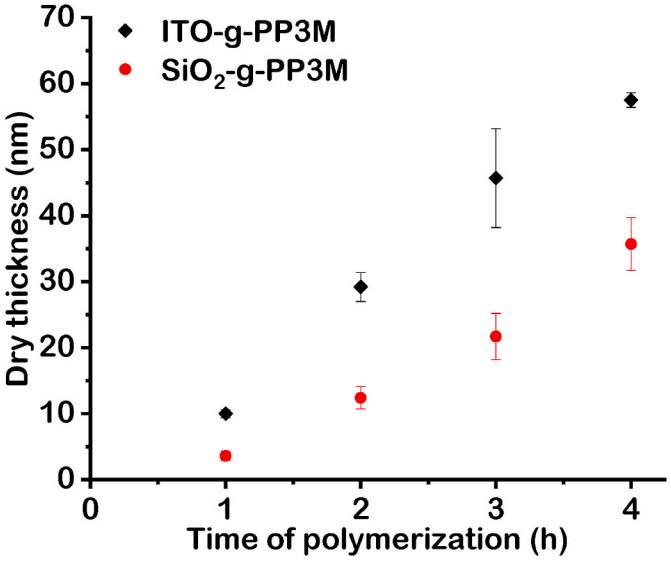

Fig. 3. Dependency of dry PP3M brushes thicknesses grafted on ITO and silicon wafers vs time of polymerization. (For interpretation of the references to colors in this figure legend, the reader is referred to the Web version of this article.)

AFM topography images captured after certain time of polymerization demonstrate gradual increase of layer thickness and formation of homogenous films (Fig. 4). However, the brush growth was faster on ITO surface with respect to silicon wafers (Fig. 3). It is worth emphasizing that the grafting densities of PP3M brushes grafted on both ITO and SiO_2 were virtually the same (see SI for details), therefore such significant differences are due to formation of longer polymer chains with higher molar masses on ITO indicating on enhancement of polymerization kinetics. We have observed similar dependency in classical SI-ATRP of methyl methacrylate and *N*-isopropylacrylamide [37]. We showed that this phenomenon is associated with release of indium and tin ions from ITO, which may then undergo redox reactions with catalyst or initiator molecules. Furthermore, it was shown that indium oxide, which is the main component of ITO, may undergo photoreduction when exposed to light of energy higher than 3eV (below 413 nm) [46], while various indium-based compounds were found to be effective photocatalyst [47]. Therefore, it is probable that in case of metal-free SI-ATRP one may expect additional activation mechanism utilizing tin or indium ions. However, the detailed investigation of that phenomenon is beyond the scope of this short communication.

PPPGs should demonstrate pH responsive behavior as nitrogen atoms in pyridine groups could be protonated in acidic solution. The most promising PP3M brushes were characterized by contact angle and AFM measurements at various pH. The apparent dissociation constant (pK_a^{app}) of PP3M grafted from silicon wafer was determined by contact angle measurements (Fig. 5). A droplet (5 μl) of hydrochloric acid solution of known pH was placed on top of the sample surface and the measurement was performed either after 2 or 5 min of incubation. It was revealed that PP3M are highly protonated only at very low pH below 1.4, while the pK_a^{app} was found to be 1.14 (see derivative curve in Fig. 5). Analogous measurements were performed for poly(methyl methacrylate) brushes (PMMA) of similar height. As expected, the contact angle values were virtually the same at each pH. It is worth emphasizing that pK_a^{app} is practically the same for both times of incubation indicating on quick protonation of the brushes in highly acidic solution. The obtained pK_a^{app} is much lower than the values observed before e.g. for P4VP in solution ($pK_a = 4$) [48]. The shifts in pK_a values in case of weak polyelectrolyte brushes compared to the same polyelectrolytes in the solution were observed previously [49,50]. This effect was related to the close proximity of the chains in the brushes. Furthermore, it was recently shown that protonation behavior of weak polyelectrolyte brushes depends very strongly on ionic strength [51]. If the protonation is realized in the presence of low salt concentration very low pH is required to protonate the polybasic brushes [51]. It is worth mentioning that pK_a^{app} of both P3VP and P4VP (polymers in solution) determined in acidic solutions without any salt (as in this work) are much lower (2.92 and 3.27) than pK_a determined in 0.1 M NaCl (5.2 and 5.1) [52].

In order to confirm such a low pK_a^{app}, the PP3M brush grafted from silicon wafer was analyzed by AFM in solutions of various pH values. PP3M obtained after 4 h of metal-free SI-ATRP was chosen for

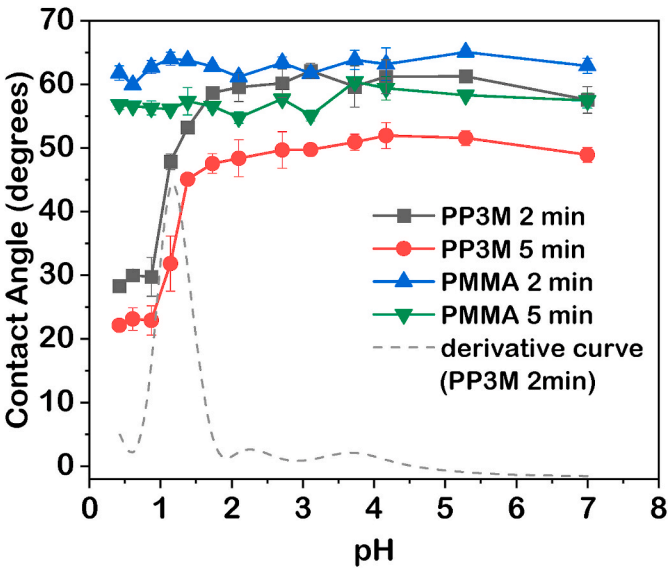

Fig. 5. Dependency of contact angles vs pH of dropped solution obtained for PP3M and reference PMMA brushes grafted from silicon wafers. The representative first derivative curve of the relationship found for PP3M (2 min incubation time) is shown as dashed line. (For interpretation of the references to colors in this figure legend, the reader is referred to the Web version of this article.)

measurements. The brush thickness was measured using special spherical probe with tip radius of 300 nm in order to reduce the penetration depth during measurements. The loading force was kept on the lowest possible level necessary to capture an accurate topography map (typically around 5 nN). The initial thickness of the brush in the dry state was equal to 37 ± 2 nm (see Fig. 6A). After immersion in deionized water or hydrochloric acid solution of pH = 3.1, insignificant swelling of the brushes was noticed as the thickness increased of only 3 nm (Fig. 6). The swelling ratio $\alpha = h_{wet}/h_{dry}$ reached 1.08 suggesting poor swelling of the layer in this condition. However, when the sample was immersed in more acidic solution of pH = 1.1 we observed a very significant increase of the layer thickness (185 ± 5 nm), while the swelling ratio reached high value $\alpha = 5.0$ (Fig. 6D). As strongly protonated and swollen PP3M brush was very soft, the layer thickness was additionally verified by capturing of nanoindentation curves at high loads (see exemplary curve in Fig. S19). The penetration depths at maximum load of 500 nN (the plots had vertical slope at this force) were in 180–190 nm range confirming the thickness measurements. It is worth emphasizing that the dry thickness of the layer after the measurement was the same as before indicating strong attachment of the PP3M chains to the silicon oxide substrate.

Weak polyelectrolyte brushes after crossing their pK_a are highly ionized and their chain extension under such conditions is driven by

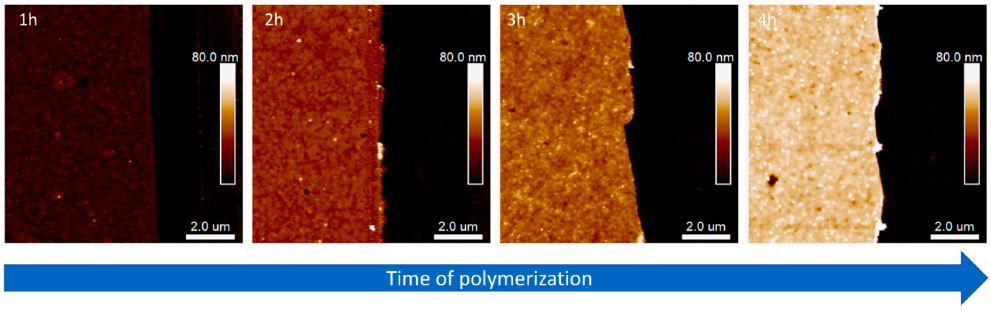

Fig. 4. AFM topography images captured at the edges of the scratch on PP3M brushes prepared after certain time of metal-free SI-ATRP on ITO substrate. The images are presented on the same height scale.

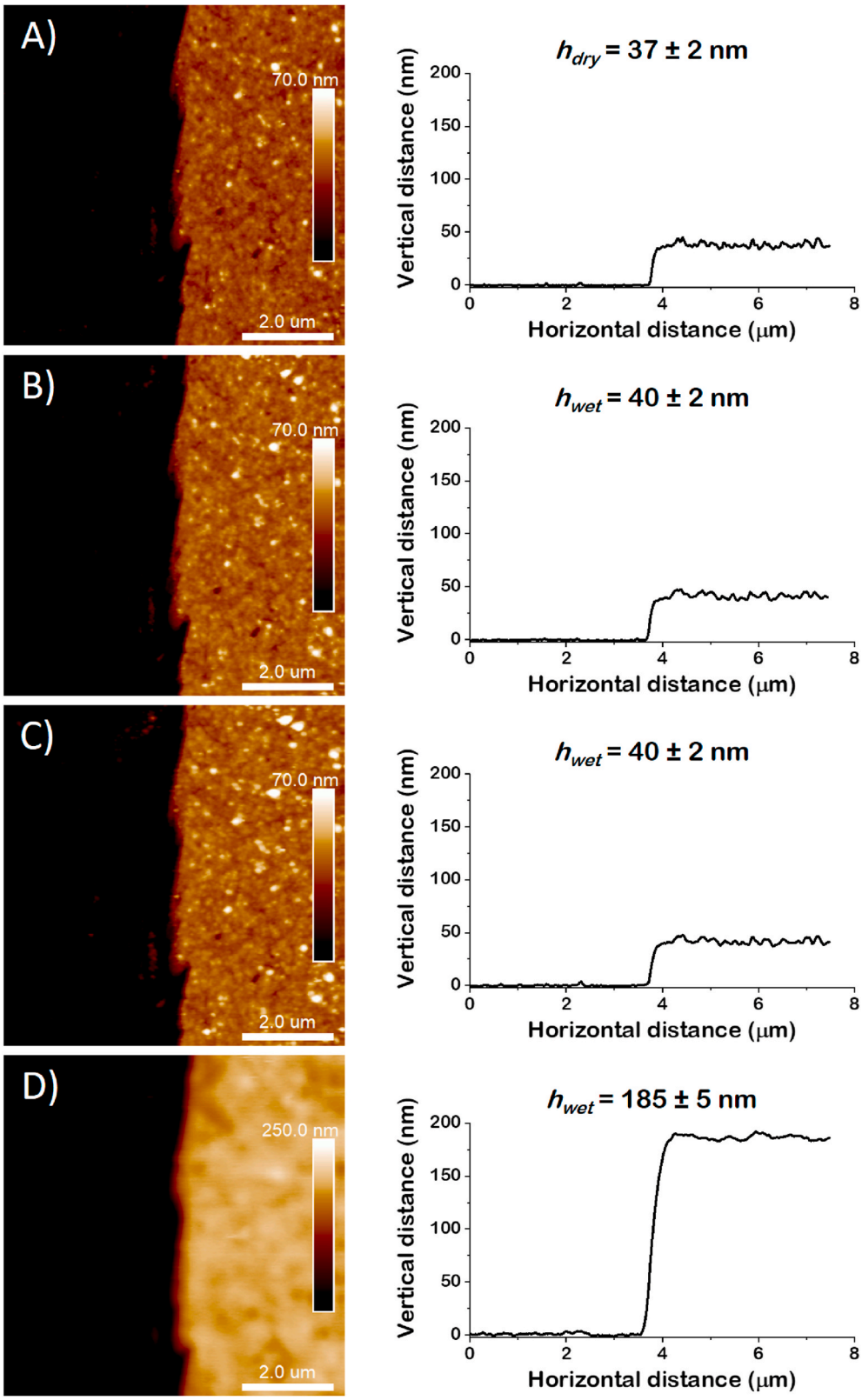

Fig. 6. AFM topography images with exemplary cross-section profiles of PP3M brush grafted from silicon substrate captured in: A) air, B) deionized water, C) hydrochloric acid solution (pH = 3.1), D) hydrochloric acid solution (pH = 1.1). (For interpretation of the references to colors in this figure legend, the reader is referred to the Web version of this article.)

both polymer and counterion osmotic pressure as well as inter-segment electrostatic repulsions [53]. As a result, the thickness of the brushes approaches the contour length of the polymer backbone [53,54]. According to that the thickness of highly protonated PP3M brush at pH = 1.1 was used for calculation of its grafting density ($\sigma = 0.23$ chains/nm^2) using the methodology described by Benetti et al. [55] (see SI for details). The obtained value was comparable to the one reported by Narupai et al. for PMMA brushes prepared by metal-free SI-ATRP ($\sigma = 0.28$ chains/nm^2) [34].

We have attempted analogous measurements for PP3M grafted from ITO (see Fig. S20) and observed negligible brush swelling in water ($\alpha = 1.03$) and hydrochloric acid solutions of pH = 3.1 ($\alpha = 1.07$) and pH = 2.0 ($\alpha = 1.05$) as well. However, when the measurement was performed at lower pH (pH = 1.1), immediate delamination of the layer was noticed pointing to degradation of ITO/brush interface (see Fig. S21). It is not surprising as HCl is a good etching agent of ITO and at high concentrations may easily react with indium ions forming indium chloride [56]. Therefore, it seems that unprotonated brush effectively blocks the degradation of the interface, while in the protonated form at low pH the acid could easily reach the interface.

4. Conclusion

In summary, we present here a facile synthetic methodology for preparation of polymer brushes with pendant pyridine groups. Three different pyridine-based monomers were synthesized and then polymerized by metal-free SI-ATRP in microliter volumes. The best performance was observed for P3M monomer with methacrylate group in meta position with respect to nitrogen atom in pyridine group. The kinetic studies revealed linear dependency of PP3M brush thickness vs polymerization time indicating controlled characteristics of metal-free SI-ATRP. The key advantages of the proposed strategy are simple reaction setup with microliter volumes of reagents and photoinitiation mechanism triggered by visible light. The performed polymerizations were conducted in air showing improved tolerance to oxygen when compared to classical ATRP, due to utilization of PTH being oxygen tolerant polymerization catalyst. The obtained brushes demonstrated pH responsive behavior associated with protonation of nitrogen atoms in PP3M in acidic solution and adoption of highly stretched conformation below pK_a. The developed methodology allows straightforward and controlled synthesis of surface-grafted PPPGs that are hardly achievable by classical ATRP with metal-based catalysts.

CRediT authorship contribution statement

Monika Słowikowska: Methodology, Investigation, Visualization, Writing – original draft. **Artur J. Wójcik:** Methodology, Investigation, Visualization, Writing – original draft. **Karol Wolski:** Conceptualization, Methodology, Investigation, Visualization, Writing – original draft, Writing – review & editing, Resources, Supervision, Funding acquisition. **Anna Hatalak:** Visualization, Investigation, Funding acquisition. **Szczepan Zapotoczny:** Conceptualization, Writing – review & editing, Resources, Supervision, Funding acquisition.

Declaration of competing interest

The authors declare that they have no known competing financial interests or personal relationships that could have appeared to influence the work reported in this paper.

Acknowledgments

This research has been supported from the Anthropocene Priority Research Area budget under the program "Excellence Initiative – Research University" at the Jagiellonian University. A. J. W. and S.Z. would like to thank for the financial support from TEAM program (grant number: TEAM/2016–1/9) of the Foundation for Polish Science co-financed by the European Union under the European Regional Development Fund. The authors would like to thank Lizaveta Fiadosava-Wójcik for creating graphical abstract as well as Paweł Chmielarz and Izabela Zaborniak for their help in GPC measurements.

Appendix A. Supplementary data

Supplementary data to this article can be found online at https://doi.org/10.1016/j.polymer.2021.124244.

References

[1] L. D'Alton, P. Nguyen, S. Carrara, C.F. Hogan, Intense near-infrared electrochemiluminescence facilitated by energy transfer in bimetallic Ir-Ru metallopolymers, Electrochim. Acta 379 (2021) 138117, https://doi.org/10.1016/j.electacta.2021.138117.
[2] D. Li, Q. He, Y. Yang, H. Möhwald, J. Li, Two-stage pH response of poly(4-vinylpyridine) grafted gold nanoparticles, Macromolecules 41 (2008) 7254–7256, https://doi.org/10.1021/ma800894c.
[3] J.G. Kennemur, Poly(vinylpyridine) segments in block copolymers: synthesis, self-assembly, and versatility, Macromolecules 52 (2019) 1354–1370, https://doi.org/10.1021/acs.macromol.8b01661.
[4] K. Wolski, M. Szuwarzyński, S. Zapotoczny, A facile route to electronically conductive polyelectrolyte brushes as platforms of molecular wires, Chem. Sci. 6 (2015) 1754–1760, https://doi.org/10.1039/c4sc04048a.
[5] A.K. Mishra, J. Lim, J. Lee, S. Park, Y. Seo, H. Hwang, J.K. Kim, Control drug release behavior by highly stable and pH sensitive poly(N-vinylpyrrolidone)-block-poly(4-vinylpyridine) copolymer micelles, Polymer 213 (2021) 1–8, https://doi.org/10.1016/j.polymer.2020.123329.
[6] J. Raczkowska, Y. Stetsyshyn, K. Awsiuk, J. Zemła, A. Kostruba, K. Harhay, M. Marzec, A. Bernasik, O. Lishchynskyi, H. Ohar, A. Budkowski, Temperature-responsive properties of poly(4-vinylpyridine) coatings: influence of temperature on the wettability, morphology, and protein adsorption, RSC Adv. 6 (2016) 87469–87477, https://doi.org/10.1039/c6ra07223b.
[7] J.G. Werner, H. Lee, U. Wiesner, D.A. Weitz, Ordered mesoporous microcapsules from double emulsion confined block copolymer self-assembly, ACS Nano 15 (2021) 3490–3499, https://doi.org/10.1021/acsnano.1c00068.
[8] S. Baek, S.R. Kwon, K. Fu, P.W. Bohn, Ion gating in nanopore electrode arrays with hierarchically organized pH-responsive block copolymer membranes, ACS Appl. Mater. Interfaces 12 (2020) 55116–55124, https://doi.org/10.1021/acsami.0c12926.
[9] H.K. Choi, D.J. Shin, S.H. Jin, K.T. Lim, S.H. Jeong, Y.S. Gal, A polyelectrolytic polyacetylene for quasi-solid state dye-sensitized solar cell applications, Mol. Cryst. Liq. Cryst. 705 (2020) 87–92, https://doi.org/10.1080/15421406.2020.1741828.
[10] G. Behzadi pour, H. Nazarpour fard, L. Fekri aval, P. Esmaili, Polyvinylpyridine-based electrodes: sensors and electrochemical applications, Ionics 26 (2020) 549–563, https://doi.org/10.1007/s11581-019-03302-z.
[11] D. Gokkaya, M. Topuzogullari, T. Arasoglu, K. Trabzonlu, M.M. Ozmen, S. Abdurrahmanoğlu, Antibacterial properties of cationic copolymers as a function of pendant alkyl chain length and degree of quaternization, Polym. Int. 70 (2021) 829–836, https://doi.org/10.1002/pi.6170.
[12] K. Zhang, L. Zong, X. Jia, Bifunctional Ru-loaded porous organic polymers with pyridine functionality: recyclable catalysts for N-formylation of amines with CO_2 and H_2, Adv. Synth. Catal. 363 (2021) 1335–1340, https://doi.org/10.1002/adsc.202001336.
[13] J.O. Zoppe, N.C. Ataman, P. Mocny, J. Wang, J. Moraes, H.A. Klok, Surface-initiated controlled radical polymerization: state-of-the-art, opportunities, and challenges in surface and interface engineering with polymer brushes, Chem. Rev. 117 (2017) 1105–1318, https://doi.org/10.1021/acs.chemrev.6b00314.
[14] F. Jiang, W.H. Meyer, J. Zhang, Dense poly(4-vinyl pyridine) brushes grafting from silica nanoparticles via atom transfer radical polymerization, Colloids Surf. A Physicochem. Eng. Asp. 436 (2013) 302–308, https://doi.org/10.1016/j.colsurfa.2013.07.005.
[15] J. Qiu, X. Zhou, Q. Mo, F. Liu, L. Jiang, Electrostatic assembled of Keggin-type polyoxometalates onto poly(4-vinylpyridine)-grafted poly(vinylidene fluoride) membranes, RSC Adv. 4 (2014) 48931–48937, https://doi.org/10.1039/c4ra07978g.
[16] J. Hu, M. Li, L. Wang, X. Zhang, Polymer brush-modified graphene oxide membrane with excellent structural stability for effective fractionation of textile wastewater, J. Membr. Sci. 618 (2021) 118698, https://doi.org/10.1016/j.memsci.2020.118698.
[17] D. Li, Y.J. Jang, J. Lee, J.E. Lee, S.T. Kochuveedu, D.H. Kim, Grafting poly(4-vinylpyridine) onto gold nanorods toward functional plasmonic core-shell nanostructures, J. Mater. Chem. 21 (2011) 16453–16460, https://doi.org/10.1039/c1jm13302k.
[18] J. Lindqvist, D. Nyström, E. Östmark, P. Antoni, A. Carlmark, M. Johansson, A. Hult, E. Malmström, Intelligent Dual-responsive cellulose surfaces via surface-initiated ATRP, Biomacromolecules 9 (2008) 2139–2145, https://doi.org/10.1021/bm800193n.
[19] L. Li, G. Yan, Z. Cheng, J. Wu, X. Yu, Q. Guo, Electroless plating of copper on Si (100) surfaces modified by surface-initiated atom-transfer radical polymerization

of 4-vinylpyridine, Surf. Interface Anal. 41 (2009) 69–74, https://doi.org/10.1002/sia.2994.
[20] J. Xia, X. Zhang, K. Matyjaszewski, Atom transfer radical polymerization of 4-vinylpyridine, Macromolecules 32 (1999) 3531–3533, https://doi.org/10.1021/ma9816968.
[21] K. Matyjaszewski, T.E. Patten, J. Xia, Controlled/'living' radical polymerization. Kinetics of the homogeneous atom transfer radical polymerization of styrene, J. Am. Chem. Soc. 119 (1997) 674–680, https://doi.org/10.1021/ja963361g.
[22] Z. Bao, M.L. Bruening, G.L. Baker, Rapid growth of polymer brushes from immobilized initiators, J. Am. Chem. Soc. 128 (2006) 9056–9060, https://doi.org/10.1021/ja058743d.
[23] J.-E. Lee, K. Chung, Y.H. Jang, Y.J. Jang, S.T. Kochuveedu, D. Li, D.H. Kim, Bimetallic multifunctional Core@Shell plasmonic nanoparticles for localized surface plasmon resonance based sensing and electrocatalysis, Anal. Chem. 84 (2012) 6494–6500, https://doi.org/10.1021/ac300654k.
[24] X. Li, X. Wei, S.M. Husson, Thermodynamic studies on the adsorption of fibronectin adhesion-promoting peptide on nanothin films of poly(2-vinylpyridine) by SPR, Biomacromolecules 5 (2004) 869–876, https://doi.org/10.1021/bm034266k.
[25] S.J. Yuan, S.O. Pehkonen, Y.P. Ting, K.G. Neoh, E.T. Kang, Inorganic-organic hybrid coatings on stainless steel by layer-by-layer deposition and surface-initiated atom-transfer-radical polymerization for combating biocorrosion, ACS Appl. Mater. Interfaces 1 (2009) 640–652, https://doi.org/10.1021/am800182d.
[26] S. Saha, M.L. Bruening, G.L. Baker, Facile synthesis of thick films of poly(methyl methacrylate), poly(styrene), and poly(vinyl pyridine) from Au surfaces, ACS Appl. Mater. Interfaces 3 (2011) 3042–3048, https://doi.org/10.1021/am200560g.
[27] J. Raczkowska, Y. Stetsyshyn, K. Awsiuk, M. Brzychczy-Włoch, T. Gosiewski, B. Jany, O. Lishchynskyi, Y. Shymborska, S. Nastyshyn, A. Bernasik, H. Ohar, F. Krok, D. Ochońska, A. Kostruba, A. Budkowski, "Command" surfaces with thermo-switchable antibacterial activity, Mater. Sci. Eng. C 103 (2019) 109806, https://doi.org/10.1016/j.msec.2019.109806.
[28] M. Słowikowska, K. Chajec, A. Michalski, S. Zapotoczny, K. Wolski, Surface-initiated photoinduced iron-catalyzed atom transfer radical polymerization with ppm concentration of Febr3 under visible light, Materials 13 (2020) 1–17, https://doi.org/10.3390/ma13225139.
[29] M. Flejszar, P. Chmielarz, K. Wolski, G. Grześ, S. Zapotoczny, Polymer brushes via surface-initiated electrochemically mediated ATRP: role of a sacrificial initiator in polymerization of acrylates on silicon substrates, Materials 13 (2020) 3559, https://doi.org/10.3390/ma13163559.
[30] W. Yan, M. Fantin, S. Ramakrishna, N.D. Spencer, K. Matyjaszewski, E.M. Benetti, Growing polymer brushes from a variety of substrates under ambient conditions by Cu0-mediated surface-initiated ATRP, ACS Appl. Mater. Interfaces 11 (2019) 27470–27477, https://doi.org/10.1021/acsami.9b09529.
[31] E.H. Discekici, C.W. Pester, N.J. Treat, J. Lawrence, K.M. Mattson, B. Narupai, E. P. Toumayan, Y. Luo, A.J. McGrath, P.G. Clark, J. Read De Alaniz, C.J. Hawker, Simple benchtop approach to polymer brush nanostructures using visible-light-mediated metal-free atom transfer radical polymerization, ACS Macro Lett. 5 (2016) 258–262, https://doi.org/10.1021/acsmacrolett.6b00004.
[32] G. Ramakers, G. Wackers, V. Trouillet, A. Welle, P. Wagner, T. Junkers, Laser-grafted molecularly imprinted polymers for the detection of histamine from organocatalyzed atom transfer radical polymerization, Macromolecules 52 (2019) 2304–2313, https://doi.org/10.1021/acs.macromol.8b02339.
[33] A. Ma, C. Jiang, M. Li, L. Cao, Z. Deng, L. Bai, W. Wang, H. Chen, H. Yang, D. Wei, Surface-initiated photoinduced electron transfer ATRP and mussel-inspired chemistry: surface engineering of graphene oxide for self-healing hydrogels, React. Funct. Polym. 150 (2020) 104547, https://doi.org/10.1016/j.reactfunctpolym.2020.104547.
[34] B. Narupai, Z.A. Page, N.J. Treat, A.J. McGrath, C.W. Pester, E.H. Discekici, N. D. Dolinski, G.F. Meyers, J. Read de Alaniz, C.J. Hawker, Simultaneous preparation of multiple polymer brushes under ambient conditions using microliter volumes, Angew. Chem. Int. Ed. 57 (2018) 13433–13438, https://doi.org/10.1002/anie.201805534.
[35] K. Targos, O.P. Williams, Z.K. Wickens, Unveiling potent photooxidation behavior of catalytic photoreductants, J. Am. Chem. Soc. 143 (2021) 4125–4132, https://doi.org/10.1021/jacs.1c00399.
[36] J. Wang, L. Yuan, Z. Wang, M.A. Rahman, Y. Huang, T. Zhu, R. Wang, J. Cheng, C. Wang, F. Chu, C. Tang, Photoinduced metal-free atom transfer radical polymerization of biomass-based monomers, Macromolecules 49 (2016) 7709–7717, https://doi.org/10.1021/acs.macromol.6b01997.
[37] A. Gruszkiewicz, M. Słowikowska, G. Grześ, A. Wójcik, J. Rokita, A. Fiocco, M. Wytrwal-Sarna, M. Marzec, B. Trzebicka, M. Kopeć, K. Wolski, S. Zapotoczny, Enhancement of the growth of polymer brushes via ATRP initiated from ions-releasing indium tin oxide substrates, Eur. Polym. J. 112 (2019) 817–821, https://doi.org/10.1016/j.eurpolymj.2018.11.004.
[38] N.J. Treat, H. Sprafke, J.W. Kramer, P.G. Clark, B.E. Barton, J. Read De Alaniz, B. P. Fors, C.J. Hawker, Metal-free atom transfer radical polymerization, J. Am. Chem. Soc. 136 (2014) 16096–16101, https://doi.org/10.1021/ja510389m.
[39] A.J. Convertine, B.S. Sumerlin, D.B. Thomas, A.B. Lowe, C.L. McCormick, Synthesis of block copolymers of 2- and 4-vinylpyridine by RAFT polymerization, Macromolecules 36 (2003) 4679–4681, https://doi.org/10.1021/ma034361l.
[40] H.C. Lee, M. Fantin, M. Antonietti, K. Matyjaszewski, B.V.K.J. Schmidt, Synergic effect between nucleophilic monomers and Cu(II) metal-organic framework for visible-light-triggered controlled photopolymerization, Chem. Mater. 29 (2017) 9445–9455, https://doi.org/10.1021/acs.chemmater.7b03541.
[41] M. Słowikowska, K. Wolski, A.J. Wójcik, D. Wesner, H. Schönherr, S. Zapotoczny, Unraveling the nanomechanical properties of surface-grafted conjugated polymer brushes with ladder-like architecture, Polym. Chem. 11 (2020) 7050–7062, https://doi.org/10.1039/d0py01422b.
[42] K. Wolski, A. Gruszkiewicz, M. Wytrwal-Sarna, A. Bernasik, S. Zapotoczny, The grafting density and thickness of polythiophene-based brushes determine the orientation, conjugation length and stability of the grafted chains, Polym. Chem. 8 (2017) 6250–6262, https://doi.org/10.1039/c7py01418j.
[43] A. Sharma, R. Kroon, D.A. Lewis, G.G. Andersson, M.R. Andersson, Poly(4-vinylpyridine): a new interface layer for organic solar cells, ACS Appl. Mater. Interfaces 9 (2017) 10929–10936, https://doi.org/10.1021/acsami.6b12687.
[44] T.K. Tam, M. Ornatska, M. Pita, S. Minko, E. Katz, Polymer brush-modified electrode with switchable and tunable redox activity for bioelectronic applications, J. Phys. Chem. C 112 (2008) 8438–8445, https://doi.org/10.1021/jp801086w.
[45] X. Pan, M. Lamson, J. Yan, K. Matyjaszewski, Photoinduced metal-free atom transfer radical polymerization of acrylonitrile, ACS Macro Lett. 4 (2015) 192–196, https://doi.org/10.1021/mz500834g.
[46] B. Pashmakov, B. Claflin, H. Fritzsche, Photoreduction and oxidation of amorphous indium oxide, Solid State Commun. 86 (1993) 619–622, https://doi.org/10.1016/0038-1098(93)90826-9.
[47] X. Zhang, D. Huang, K. Xu, D. Xu, F. Liu, S. Zhang, Indium-containing visible-light-driven (VLD) photocatalysts for solar energy conversion and environment remediation, in: Semicond. Photocatal. - Mater. Mech. Appl., 2016, https://doi.org/10.5772/63233.
[48] M. Satoh, E. Yoda, T. Hayashi, J. Komiyama, Potentiometric titration of poly (vinylpyridines) and hydrophobic interaction in the counterion binding, Macromolecules 22 (1989) 1808, https://doi.org/10.1021/ma00194a051.
[49] L. Franck-Lacaze, P. Sistat, P. Huguet, Determination of the pKa of poly (4-vinylpyridine)-based weak anion exchange membranes for the investigation of the side proton leakage, J. Membr. Sci. 326 (2009) 650–658, https://doi.org/10.1016/j.memsci.2008.10.054.
[50] N. Schüwer, H.-A. Klok, Tuning the pH sensitivity of poly(methacrylic acid) brushes, Langmuir 27 (2011) 4789–4796, https://doi.org/10.1021/la200347u.
[51] G. Ferrand-Drake Del Castillo, R.L.N. Hailes, A. Dahlin, Large changes in protonation of weak polyelectrolyte brushes with salt concentration-implications for protein immobilization, J. Phys. Chem. Lett. 11 (2020) 5212–5218, https://doi.org/10.1021/acs.jpclett.0c01289.
[52] J.D. Roach, M.M. Bondaruk, A. Al-Abdulghani, Z. Shahrori, Counterion binding in aqueous solutions of poly(vinylpyridines) as assessed by potentiometric titration, Adv. Mater. Phys. Chem. 6 (2016) 249–261, https://doi.org/10.4236/ampc.2016.69025.
[53] D. Iqbal, J. Yan, K. Matyjaszewski, R.D. Tilton, Swelling of multi-responsive spherical polyelectrolyte brushes across a wide range of grafting densities, Colloid Polym. Sci. 298 (2020) 35–49, https://doi.org/10.1007/s00396-019-04585-4.
[54] J.K. Riley, K. Matyjaszewski, R.D. Tilton, Electrostatically controlled swelling and adsorption of polyelectrolyte brush-grafted nanoparticles to the solid/liquid interface, Langmuir 30 (2014) 4056–4065, https://doi.org/10.1021/la500570u.
[55] E.M. Benetti, S. Zapotoczny, G.J. Vancso, Tunable thermoresponsive polymeric platforms on gold by "photoiniferter"-based surface grafting, Adv. Mater. 19 (2007) 268–271, https://doi.org/10.1002/adma.200601554.
[56] C.J. Huang, Y.K. Su, S.L. Wu, The effect of solvent on the etching of ITO electrode, Mater. Chem. Phys. 84 (2004) 146–150, https://doi.org/10.1016/j.matchemphys.2003.11.021.